Hydrol. Earth Syst. Sci. Discuss., 11, 13259–13309, 2014
www.hydrol-earth-syst-sci-discuss.net/11/13259/2014/
doi:10.5194/hessd-11-13259-2014

Hydrology and Earth System Sciences
Open Access
Discussions

From runoff to rainfall: inverse rainfall–runoff modelling in a high temporal resolution

M. Herrnegger, H. P. Nachtnebel, and K. Schulz

Institute of Water Management, Hydrology and Hydraulic Engineering, University of Natural Resources and Life Sciences, Vienna, Austria

Received: 16 November 2014 – Accepted: 19 November 2014 – Published: 5 December 2014

Correspondence to: M. Herrnegger (mathew.herrnegger@boku.ac.at)

Published by Copernicus Publications on behalf of the European Geosciences Union.

Abstract

This paper presents a novel technique to calculate mean areal rainfall in a high temporal resolution of 60 min on the basis of an inverse conceptual rainfall–runoff model and runoff observations.

Rainfall exhibits a large spatio-temporal variability, especially in complex alpine terrain. Additionally, the density of the monitoring network in mountainous regions is low and measurements are subjected to major errors, which lead to significant uncertainties in areal rainfall estimates. The most reliable hydrological information available refers to runoff, which in the presented work is used as input for a rainfall–runoff model. Thereby a conceptual, HBV-type model is embedded in an iteration algorithm. For every time step a rainfall value is determined, which results in a simulated runoff value that corresponds to the observation. To verify the existence, uniqueness and stability of the inverse rainfall, numerical experiments with synthetic hydrographs as inputs into the inverse model are carried out successfully. The application of the inverse model with runoff observations as driving input is performed for the Krems catchment (38.4 km^2), situated in the northern Austrian Alpine foothills. Compared to station observations in the proximity of the catchment, the inverse rainfall sums and time series have a similar goodness of fit, as the independent INCA rainfall analysis of Austrian Central Institute for Meteorology and Geodynamics (ZAMG). Compared to observations, the inverse rainfall estimates show larger rainfall intensities. Numerical experiments show, that cold state conditions in the inverse model do not influence the inverse rainfall estimates, when considering an adequate spin-up time. The application of the inverse model is a feasible approach to obtain improved estimates of mean areal rainfall. These can be used to enhance interpolated rainfall fields, e.g. for the estimation of rainfall correction factors, the parameterisation of elevation dependency or the application in real-time flood forecasting systems.

HESSD

11, 13259–13309, 2014

1 Introduction

Areal or catchment rainfall estimates are fundamental for many hydrological problems, as they represent an essential input for modelling hydrological systems. They are however subject to manifold uncertainties, since it is not possible to observe the mean catchment rainfall itself (Sugawara, 1992; Valéry et al., 2009). Catchment rainfall values are therefore generally estimated by interpolation of point measurements, sometimes incorporating information on the spatial rainfall structure from remote sensing, e.g. radar (e.g. Haiden et al., 2011). Measurement, sample and model errors can be identified as sources of uncertainty. Point observations of rainfall, which are the basis for the calculation of mean areal rainfall values, are error inflicted (Sevruk, 1981, 1986; Sevruk and Nespor, 1998; Seibert and Moren, 1999; Wood et al., 2000; Fekete et al., 2004). Occult precipitation forms like fog or dew are frequently ignored. Although not generally relevant, this precipitation form can be a significant contribution to the water budget of a catchment (Elias et al., 1993; Jacobs et al., 2006; Klemm and Wrzesinsky, 2007). The highest systematic measurement errors of over 50 % are found during snowfall in strong wind conditions. Other sources of measurement errors and their magnitudes are listed in Table 1.

In complex terrain the rainfall process is characterised by a high temporal and spatial variability. Especially in these areas the density of the measurement network tends to be low, not capturing the high variability and leading to sample errors (Wood et al., 2000; Simoni et al., 2011; de Jong et al., 2002). Further uncertainties arise in the interpolation of catchment scale rainfall from point observations. Systematic and stochastic errors of the regionalisation methods can be identified (model errors). Systematic model errors can arise during the regionalisation of rainfall in alpine areas, when e.g. the elevation dependency is not considered (Haiden and Pistotnik, 2009). Quantitative areal rainfall estimates from radar products are, although they contain precious information on the rainfall structure, still afflicted with significant uncertainties (Krajewski et al., 2010; Krajewski and Smith, 2002). A general magnitude of overall uncertainty,

HESSD
11, 13259–13309, 2014

which arises during the generation of areal rainfall fields, is difficult to assess, as different factors, e.g. topography, network density or regionalisation method, play a role.

Errors in runoff measurements are far from negligible (Di Baldassarre and Montanari, 2009; McMillan et al., 2010; Pappenberger et al., 2006; Pelletier, 1987). When applying the rating-curve method for estimation of river discharge the uncertainties are a function of the quality of the rating curve and the water level measurements. The quality of the rating curve depends on (i) the quality and stability of the measured cross-section over time, (ii) the representativeness of the velocity measurements and (iii) the influence of steady and unsteady flow conditions. According to literature the overall uncertainty, at the 95 % confidence level, can vary in the range of 5–20 % (Di Baldassarre and Montanari, 2009; Pelletier, 1987). Although it can be expected, that the measurement error will certainly be large during flood events due to its dynamic features, the errors are considerable lower compared to rainfall measurements and to the uncertainties introduced when calculating mean areal rainfall. It must however be assumed, that transboundary flows and groundwater flows around the gauging station are small and can therefore be neglected. In this paper we therefore present and explore a method to estimate catchment rainfall from runoff observations in a high temporal resolution of 60 min on the basis of a HBV-type conceptual hydrological model.

A classical application of hydrology, the problem of reproducing observed runoff with meteorological forcings as input through a formalised representation of reality, is a forward or direct problem. Two inverse problems can be identified with the forward problem (Groetsch, 1993):

1. causation problem: determination of input I (= cause), with given output O (= effect) and given model K, including model parameters θ (= process);
2. model identification problem: determination of model K, given input I and output O.

The model identification problem can be divided into (i) the problem of identifying the model structure itself and (ii) the determination of model parameters that characterise

HESSD
11, 13259–13309, 2014

the system (Tarantola, 2005). The focus in this contribution lies in solving the causation problem, i.e. in the determination of rainfall input from runoff, with a given model structure. In the following, the model, which calculates mean catchment rainfall values from runoff, will be called inverse model. The conventional model, which uses rainfall and potential evapotranspiration as input to calculate runoff, will be called forward model.

Runoff from a closed catchment is the integral of rainfall over a certain period, considering evapotranspiration losses and water storage characteristics within the catchment. Therefore, runoff observations can be used to derive information on rainfall. This has been done in several studies (e.g. Bica et al., 2011; Valéry et al., 2009, 2010; Ahrens et al., 2003; Jasper and Kaufmann, 2003; Kunstmann and Stadler, 2005; Jasper et al., 2002). The common basis of these studies was to indirectly gain information on catchment rainfall by comparing simulated runoff results with observations. Hino and Hasabe (1981) fitted an AR (autoregressive) model to daily runoff data, while assuming rainfall to be white noise. By inverting the AR model they directly generated time series of rainfall from runoff. Vrugt et al. (2008) and Kuczera et al. (2006) derived rainfall multipliers or correction factors from stream flow with the DREAM- and BATEA-methods, these methods however being computationally intensive. In a well-received study, Kirchner (2009) analytically inverted a single-equation rainfall–runoff model to directly infer time series of catchment rainfall values from runoff. Krier et al. (2012) applied the model of Kirchner (2009) to 24 small and mesoscale catchments in Luxembourg to generate areal rainfall. No systematic differences in the quality of the rainfall estimates are found between different catchment sizes. In periods with higher soil moisture the rainfall simulations show a higher performance, which is explained by the fact, that wet catchments are more likely to react as simple dynamical systems. The parsimonious approach of Kirchner (2009) is however limited to catchments, in which discharge is determined by the volume of water in storage.

Also due to the larger number of model parameters and thus higher degrees of freedom and flexibility in the calibration procedure, HBV-type conceptual models in contrary can be applied to catchments with a wider range of runoff characteristics (Bergström,

HESSD
11, 13259–13309, 2014

1995; Kling et al., 2015; Kling, 2006; Perrin et al., 2001). Therefore, in this study, the conceptual rainfall–runoff model COSERO (Nachtnebel et al., 1993; Eder et al., 2005; Kling and Nachtnebel, 2009; Herrnegger et al., 2012; Kling et al., 2015, among others), which in its structure is similar to the HBV-model, is used as a basis for the inverse model. The COSERO model has been frequently applied in research studies, but also engineering projects (see Kling et al., 2015 for details).

This paper is organized as follows: following this introduction the methods-section describes the conventional conceptual rainfall–runoff model (forward model), the inverse model and the virtual experiments to verify the existence, uniqueness and stability of the inverse rainfall simulations. The inverse model is applied to a catchment in the foothills of the northern Austrian Alps. The catchment and the data base is presented. The parameter calibration and validation of the forward model is described in the results and discussion section. Here also different results of the inverse model are described and discussed: apart from results from the calibration and validation period the influence of different calibration inputs and system states on the inverse rainfall estimates are presented. Finally the paper ends with a summary and conclusions.

2 Methods

2.1 Forward model (rainfall–runoff model)

In the continuous forward model, the unknown runoff Q_t is a function f of known variables rainfall input R_t, potential evapotranspiration ETp_t, system states S_{t-1} and a set of model parameters θ_i, whereas the index t denotes time:

$$Q_t = f(R_t, \mathrm{ETp}_t, S_{t-1}, \theta_i). \quad (1)$$

The rainfall–runoff model used is based on the COSERO model (see introduction for references). It includes an interception and soil module and three reservoirs for

HESSD
11, 13259–13309, 2014

interflow, base flow and routing. The model structures is shown in Fig. 1, model parameters in Table 2 and fluxes and system states in Table 3.

The COSERO-model is formulated in a state space approach, with state transition functions

$$S_t = f(S_{t-1}, I_t) \tag{2}$$

and output functions

$$O_t = f(S_{t-1}, I_t) \tag{3}$$

with

I_t Input (mm/Δt), e.g. rainfall (Table 2)

O_t Output (mm/Δt), e.g. total runoff (Table 2)

S_t System states (mm), e.g. water stored in soil module (Table 2).

These functions have a time component, which is indicated by the index "t". Schematically the state space approach can be represented as shown in Fig. 2.

The model formulation can be found in the Appendix.

2.2 Inverse model (runoff-rainfall model)

In the inverse model the unknown rainfall R_t is a function of runoff Q_t, potential evapotranspiration ETp_t, system states S_{t-1} and a set of model parameters θ_i, whereas the index t denotes time:

$$R_t = f^{-1}(Q_t, \mathrm{ETp}_t, S_{t-1}, \theta_i). \tag{4}$$

The chief objective in the application of the inverse model is the estimation of rainfall from observed runoff. The forward model is embedded in an iteration algorithm,

HESSD
11, 13259–13309, 2014

in which for every time step t the rainfall value R_t is determined, which satisfies the function

$$f(R_t) = \mathrm{QSIM}_t(R_t, \mathrm{ETp}_t, S_{t-1}, \theta_i) - \mathrm{QOBS}_t \leq \varepsilon \quad (5)$$

with

$$R_{t,\min} \leq R_t < R_{t,\max}. \quad (6)$$

The upper and lower brackets of rainfall ($R_{t,\min}$ and $R_{t,\max}$) is set to 0 and 50 mm h^{-1}. QSIM_t and QOBS_t is the simulated and observed runoff. ε denotes a small value, which is ideally zero. The determined rainfall value R_t represents the "best" simulated rainfall of the catchment and can also be used as input into the forward model to simulate runoff. Therefore for every time step the inverse model simulates a rainfall and a corresponding runoff value. The simulated runoff value should ideally be identical to the observed value. This is however not always the case, as will be shown later. A more elegant method to calculate rainfall from runoff by analytically inverting the model equations is principally possible, but has some disadvantages (Herrnegger, 2013).

Solving Eq. (5) is basically a root finding problem. Different root finding algorithms were therefore tested, with the Van Wijngaarden–Dekker–Brent Method (Brent, 1973; Press et al., 1992) being the method of choice, as this method exhibited the fastest and most robust results. The Brent's method combines root bracketing, bisection and invers quadratic interpolation to converge from the neighbourhood of a zero crossing and will always converge, as long as the function can be evaluated within the initial defined interval (in our case $R_{t,\min}$ and $R_{t,\max}$) known to contain a root (Press et al., 1992). The iteration progress for one model time step is illustrated in Fig. 3. The left y axis shows the objective function values, the right y axis (in logarithmic scale) the associated rainfall values estimated during the iteration procedure.

HESSD
11, 13259–13309, 2014

Limitations of the inverse model

It is assumed that all runoff from the catchment passes through the measurement cross section of the gauging station. Subsurface and transboundary flows are assumed to be negligible.

The inverse model is based on a lumped model setup. Therefore the resulting inverse rainfall value corresponds to the mean areal rainfall. Applying a spatially distributed model is not possible, since the origin of outputs of different zones or cells of a distributed model setup cannot be reproduced by the inverse model in a deterministic way without additional information. The information of origin gets lost as soon as cell values are summed and routed to a catchment runoff value.

The inverse model can only be applied in snow free catchments or periods without snow. Snow models accumulate snow in a "reservoir without memory", as solid rainfall is accumulated without the information of point in time. It is therefore impossible to invert snow models.

2.3 Virtual experiments

The preconditions of existence, uniqueness and stability of the inverse rainfall values are evaluated with virtual experiments. Very small errors resulting from numerical issues in single modules, e.g. the soil layer, propagate through the model cascade and can be amplified, leading to erroneous results. As the model is formulated in a state-space approach, outputs are also dependent on the system states of a given time step. It is therefore quite conceivable, that a combination of different system states can lead to identical realisation of rainfall results. Finally, an inverse rainfall value calculated in one time step directly influences the system states for the next time step. Erroneous inverse rainfall values can therefore lead to unstable results. For the virtual experiments, runoff simulations are performed with the forward models driven with observed rainfall as input. The simulated runoff time series of the forward models are then used as input into the inverse model, with the aim to reproduce the observed rainfall originally

HESSD
11, 13259–13309, 2014

used as driving input in the forward model. Simulated runoff from the forward model is dependent on the model parameters. Therefore, to test the inversion procedure for the whole parameter range, synthetic hydrographs are produced with Monte Carlo simulations. 20 000 different parameter combinations are chosen randomly from the parameter space, with the same number of model runs to evaluate the inverse model. The sampled parameters and associated range is shown in Table 2. The schematic setup of the virtual experiment and the evaluation of the inverse model is shown in Fig. 4. Note, that the setup and the evaluation is performed for every individual Monte Carlo run, as the simulated runoff from the forward model varies, depending on selected model parameters.

The virtual experiments enable a rigorous evaluation of the inverse calculations, neglecting uncertainties concerning measurement errors in runoff, model structure or model parameters. All system states, variables and fluxes of the forward model are perfectly known at every point in time. This information is used to evaluate the inverse models. Only after a successful evaluation of the inverse model with the virtual experiments, can observations of runoff be used as input into the inverse models.

2.4 Model calibration and simulations with observed rainfall as input

Parameter calibration is performed for the forward model, using the Shuffled Complex Evolution Algorithm (Duan et al., 1992) to automatically optimise model parameters. As an optimisation criterion the widely used Nash–Sutcliffe-Efficiency (NSE, Nash and Sutcliffe, 1970) was chosen. The optimised parameters are used in the inverse model to calculate rainfall from observed runoff (Fig. 5).

To evaluate the influence of model parameters on the inverse rainfall, 2 different data sets of observed rainfall are used as calibration input in the forward model, resulting in 2 different parameters sets for simulating inverse rainfall. Model parameters are also evaluated in independent validation periods.

HESSD
11, 13259–13309, 2014

3 Materials

3.1 Study area

The Krems catchment is located about 170 km south-west of the Austrian capital of Vienna at the foothills of the Northern Alps and covers an area of 38.4 km^2 with a mean elevation of 598 m a.s.l. (Table 4, Fig. 6). Approximately 46 % of the area is covered by grassland and meadows, 48 % by mixed forest, 4 % by settlements and 2 % by coniferous forest. Mean annual rainfall amounts to 1345 mm, with a mean annual runoff of 1.12 $m^3 s^{-1}$ (Table 4). On a long term basis the highest runoff can be expected during snow melt in spring, the lowest runoff in summer and autumn until October.

3.2 Meteorological database

Two different rainfall time series are used. Ground observations of rainfall are available from the station Kirchdorf located at the catchment outlet (Fig. 6). For additional evaluation of the rainfall calculated by the inverse model, areal rainfall data from the INCA system (Integrated Nowcasting through Comprehensive Analysis; Haiden et al., 2011) is used. INCA is the operational nowcasting and analysis application developed and run by the Central Institute for Meteorology and Geodynamics of Austria (ZAMG), which is also used for the majority of real-time flood forecasting systems in Austria (Stanzel et al., 2008). For the presented study analysis fields derived from observations, but no nowcasting fields, are used. Rainfall in INCA is determined by a nonlinear spatial interpolation of rain-gauge values, in which the radar field is used as a spatial structure function. In addition an elevation correction is applied (Haiden and Pistotnik, 2009). The stations used for the interpolation of the INCA-rainfall fields are shown as triangles in Fig. 6. Note, that the station Kirchdorf is not included in the INCA analysis. The rainfall fields from the INCA system cover the test basins in a spatial resolution of 1 km^2. From the spatial data set mean catchment rainfall values are obtained by calculating area-weighted means from the intersecting grid cells.

HESSD
11, 13259–13309, 2014

Potential evapotranspiration input is calculated with the temperature and potential radiation method of Hargreaves (Hargreaves and Samani, 1982).

3.3 Simulation periods

All simulations are performed with a temporal resolution of 60 min. The virtual experiments are performed for a period of 4.5 months (15 May 2006–30 September 2006) resulting in 3336 time steps being evaluated. Calibration of the model parameters is carried out for the years 2006 to 2008. Data from the year 2009 is used for validation purposes. Only the months June, July, August and September are evaluated, as only in these months it can be guaranteed, that no snow melt contribution influences runoff. Rainfall time series for calibration and validation from the station Kirchdorf are used. Additional tests of the inverse model are performed using the INCA-data as calibration input.

4 Results and discussions

4.1 Virtual experiments

In the virtual experiments it could be proven, that the precondition of existence, uniqueness and stability of the inverse model results is given. Using all 20 000 simulated hydrographs from the Monte Carlo runs, where the parameters were varied stochastically, the observed rainfall time series could be identically reproduced by the inverse model. Apart from the rainfall also all system states and model variables where identical in the forward and inverse model runs. Results from the virtual experiments are documented in Herrnegger (2013).

HESSD
11, 13259–13309, 2014

4.2 Parameter calibration and validation of the forward model

A precondition for the application of the inverse model is that the observed runoff characteristics of the catchment are reproduced reasonably by the forward model, since these parameters are also used in the inverse model. The following section therefore shortly presents the runoff simulations of the forward model, based on the model parameters optimised with the rainfall time series of the station Kirchdorf as input.

The model performance for the calibration period of the forward model, expressed by Pearson's correlation (CORR) and Nash–Sutcliffe-Efficiency (NSE), is shown in Fig. 7.

The correlation between simulated and observed runoff in different years lies between 0.89 and 0.95. The NSE values range from 0.78 and 0.89. Evaluating all relevant months (June, July, August and September) for the period 2006–2008 yields an overall correlation of 0.92 and a NSE-value of 0.84. It can be concluded that the model performance within the years is fairly stable and comparable.

Generally, the dynamics and variability of the runoff observations are reproduced in a satisfactory manor by the forward model (Fig. 8). Although there is a tendency of underestimating runoff observations as indicated by the regression line, no obvious systematic errors are visible from the scatter plot (Fig. 9).

The validation of the forward model yields good results. In the year of 2009 a NSE of 0.86 and a correlation value of 0.93 is obtained. Thus, the model efficiency is comparable to the calibration period.

The simulations are performed with a lumped model setup. Consequently heterogeneity in geology and land use within the catchment are not explicitly considered in the parameter estimation. Taking this into consideration, it can be concluded that the general responses of the catchment to rainfall input are captured appropriately by the forward model. It is therefore justified to calculate areal rainfall from runoff using the inverted forward model, including the optimised parameters.

HESSD
11, 13259–13309, 2014

4.3 Inverse model

4.3.1 Calibration period

For the evaluation of the simulated rainfall from the inverse model (Inverse P) we will compare the calculated values with observed data of the Kirchdorf station (POBS) and the rainfall values from the INCA-system (INCA). The ground observation is not used in in the interpolation process for the INCA-rainfall fields, as it belongs to a monitoring network operated by a different institution (see Fig. 6). Generally the inverse rainfall results are presented with cumulative rainfall diagrams, scatterplots, time series plots and different objective performance criteria.

The cumulative curves of the different rainfall realisations (Fig. 10) show very similar temporal dynamics. Although large deviations are sometimes evident, the deviations of the cumulative curves of INCA and inverse rainfall (Inverse P) from the cumulative curves of the ground observation (POBS) are generally of similar magnitude. For the months June and July in 2006 the cumulative sum of the inverse rainfall for example follows POBS more closely compared to the INCA-data set. Around the 1 August 2006 a period of higher runoff was observed in the catchment (Fig. 8). During this event higher rainfall compared to POBS was simulated by the inverse model, explaining the stronger increase in the inverse rainfall sum during this period. As a results the inverse rainfall sum converges towards the INCA data.

For the period in 2007 the cumulative inverse rainfall sums agree very well with the curve of POBS. In this year the deviations of the INCA-data from POBS are higher. In the period of 2008 the deviation of the inverse rainfall sums from POBS data are slightly higher compared to INCA data. On the basis of the different cumulative rainfall sums it can therefore be concluded, that on a longer temporal basis the inverse model is capable of simulating the catchment rainfall from runoff observations.

The scatterplots in Fig. 11 show the relationships between the different rainfall realisations for 1 h, and aggregated 6 and 24 h rainfall sums. Note, that the hourly data corresponds to the modelling time step. The relationships between ground observation

HESSD
11, 13259–13309, 2014

and inverse rainfall (POBS – Inverse P) are shown in Fig. 11a–c. In the second row ground observation vs. INCA-rainfall (POBS – INCA; Fig. 11d–f) are shown.

It can be summarised:

In the POBS – Inverse P case (Fig. 11a–c) the monitored rainfall data are in many cases lower, especially for 1 h sums. For some observed high rainfall intensities, the inverse model yields no or very low rainfall intensities. This occurs in periods, in which simulated runoff from the inverse model is larger than observed runoff, as no rainfall is estimated in the inverse model.

In the POBS – INCA case (Fig. 11d–f) the INCA data yields lower values than observations, especially for higher intensities in the 1 h sums, but also for longer time intervals. The INCA interpolation method obviously smoothes the rainfall field with a high temporal resolution. It is noticeable, that for some point observations with no or little rainfall, INCA predicts rainfall. This is explained by the relative large mean distance between the stations used for the INCA-interpolation and the catchment, which is about 17 km.

Especially for the hourly data a large scatter around the 1 : 1 line is found for both cases, also explaining the low coefficient of determination (R^2) values.

Generally, for longer time intervals $\Delta t \geq 6$ h all datasets are in good agreement.

Compared to INCA, the coefficient of determination (R^2) between observed data and inverse rainfall is slightly higher ($R^2 = 0.24$ vs. $R^2 = 0.18$, Fig. 11a and d). For the 6 and 24 h sums similar coefficients of determination, which are considerably higher compared to the 1 h sums, are calculated (Fig. 11b and e; Fig. 11c and f).

The model performance expressed by the correlation coefficient is used to measures the models ability to reproduce timing and shape of observed values. It is independent of a possible quantitative bias. In the introduction the difficulties involved in the quantitative measurement of rainfall were discussed. It can, however, be assumed that a qualitative measurement, e.g. if it rains or not, will be more reliable. Figure 12 shows the correlation values between ground observation and inverse rainfall (POBS – Inverse

HESSD
11, 13259–13309, 2014

P) and ground observation and INCA rainfall (POBS – INCA) for different periods and temporal aggregation lengths.

The correlation values between ground observations and inverse rainfall and INCA increase with temporal aggregation levels. The correlation between ground observations and inverse rainfall is higher or of the same magnitude compared to the correlation between ground observation and INCA rainfall. An exception is seen here for the year 2007, where the correlation between POBS and inverse P is considerably lower compared to POBS and INCA.

Figure 13 shows the mean squared error (MSE) between ground observation and INCA (POBS – INCA) and ground observation and inverse rainfall (POBS – Inverse P) for temporal aggregation lengths of 1 h (Fig. 13a), 6 h (Fig. 13b) and 24 h (Fig. 13c). With ground observations as a basis, the evaluation with the correlation coefficient suggests that the quality of the temporal dynamics of the rainfall values from the inverse model is similar or better, compared to INCA. In contrast, the MSE between inverse and observed rainfall is generally higher compared to POBS and INCA and exhibits a higher variability in the single years.

Compared to ground observations and INCA the variance of the inverse rainfall is considerably higher for all aggregation lengths and periods (Fig. 14a–c). Although the rainfall sums of the individual years are very similar (Fig. 10), the higher variance leads to higher MSE-values of the inverse rainfall compared to observed rainfall. The variance of POBS and INCA is mostly very similar, explaining the comparatively lower MSE-values between POBS and INCA.

Figure 15 exemplarily illustrates the temporal development of the different rainfall realisations and runoff simulations for the highest flood event in the simulation period. Compared to the ground observation POBS and INCA the inverse rainfall exhibits a higher variability and higher intensities. The higher variability and oscillating nature of the inverse rainfall is explainable with the reaction of the inverse model to small fluctuations in runoff observations: in case of rising runoff observations, rainfall will be estimated by the inverse model. If the observed runoff decreases and the simulated runoff

HESSD
11, 13259–13309, 2014

of the inverse model is larger than observed runoff, no inverse rainfall will be calculated, leading to the visible oscillations. Figure 15b shows, that the forward model, driven with POBS as input, underestimates both flood peaks. The forward model, driven with the inverse rainfall, simulates both peaks very well (Inverse QSIM). However, especially the falling limb after the second flood peak on the 7 September is overestimated by the inverse model. In this period it is also visible, that no rainfall is calculated by the inverse model.

For a given time interval, the inverse model will yield an exact agreement between observed and simulated runoff, as long as there is a positive rainfall value R_t to solve Eq. (5). This will be the case in periods of rising limbs of observed runoff (driven periods), as a rainfall value can be estimated, which raises the simulated runoff value to match observation. On the contrary, in periods of observed falling limbs (non-driven periods) the simulated runoff will solely be a function of the model structure, its parameters and the antecedent system states, as negative rainfall values are ruled out beforehand. This explains, why in periods, in which the simulated runoff is higher than the observed value, no rainfall is calculated by the inverse model.

4.3.2 Validation period

It can be argued, that the inverse rainfall is conditioned by the model parameter set from the calibration period, since the inverse rainfall shown in the preceding section was simulated with these parameters. The conclusion would be, that the performance of the inverse model to estimate rainfall in an independent period will deteriorate. This objection is absolutely legitimate, since model performance in classical rainfall–runoff modelling frequently deteriorates in independent validation periods. The following results therefore show the inverse rainfall calculation for the independent validation period in the year 2009. The cumulative curves for the different rainfall realisations (Fig. 16) show a very similar behaviour compared to the data of 2006 to 2008 (see Fig. 10). Although there is a considerable deviation between the inverse rainfall and POBS curve at the end of the simulation period, the inverse rainfall matches quite well with the INCA

HESSD
11, 13259–13309, 2014

data. This behaviour is very comparable to the year 2006 in the calibration period (see Fig. 10).

The correlation values between POBS and Inverse P in the validation period shown in Fig. 17 are comparable to the values of the calibration period (see Fig. 11). No obvious deterioration of the model performance is evident, leading to the conclusion that the model parameters where not strongly conditioned by the runoff conditions in the calibration period.

4.3.3 Influence of different parameter optimisation data basis

The model parameters used for the forward and inverse model were automatically calibrated using the ground observation POBS as input. It could therefore be concluded that the model parameters are conditioned by POBS and that in consequence the good agreement between POBS and inverse P originates from this conditioning. Based on this hypothesis, calibrating the model with INCA data should lead to a better agreement between the INCA data and the corresponding inverse rainfall and a deterioration of the correlation between station data and inverse rainfall. To test this hypothesis, the forward model was automatically calibrated with INCA data as input and the resulting parameters set was then used to calculate the inverse rainfall. Based on the results shown in Fig. 18 this hypothesis can however be rejected. Although the correlation values between POBS and inverse P based on the POBS as calibration input are slightly higher compared to the inverse P values based on the INCA data calibration, the correlation values between INCA and the two different Inverse P realisations do not show noticeable differences.

It can therefore be concluded that agreement between POBS and inverse P is of similar magnitude, when simulating catchment rainfall with model parameters calibrated with the INCA data as input. This excludes that the parameters are conditioned by the input used for calibration.

HESSD
11, 13259–13309, 2014

4.3.4 Influence of cold system states on the inverse rainfall

Given the model structure, the inverse rainfall is a function of observed runoff, potential evapotranspiration, system states and model parameters (see Eq. 4). Extending Eq. (4) explicitly with all relevant system states (see Table 4) leads to

$$R_t = f^{-1}(Q_t, \mathrm{ETp}_t, \mathrm{BWI}_{t-1}, \mathrm{BW1}_{t-1}, \mathrm{BW2}_{t-1}, \mathrm{BW3}_{t-1}, \mathrm{BW4}_{t-1}, \theta_i). \quad (7)$$

Given Eq. (7) it is conceivable, that the inverse rainfall R_t may be over-determined, meaning that different combinations of system states BW_i can lead to the same inverse rainfall estimates and that the results would not be unique. The forward and inverse models are run as a continuous simulation in time (Fig. 2). The preceding system states are therefore an integral part of the simulation and are determined intrinsically within the simulation. However, the initial system states at the beginning of the simulation period (cold states) will influence the results of the simulation, but should, after an adequate spin-up time, not influence the inverse rainfall estimates. To evaluate the influence of cold states on the inverse rainfall a virtual experiment was set up, in which 3 different cold start scenarios where defined:

- reference scenario,
- dry system states scenario,
- wet system states scenario.

For the reference scenario the system states of the 31 December 2008 from the continuous simulation were used. For the cold states in the dry scenario the states from the reference scenario where reduced by the factor 0.5 and increased by the factor 1.5 for the wet scenario.

From Fig. 19 showing the monthly rainfall sums of the different model runs it is evident, that the inverse rainfall calculations differ significantly at the beginning of the simulation. The simulations were performed in a temporal resolution of 60 min, and

HESSD
11, 13259–13309, 2014

only the results aggregated to monthly values for visualisation purposes. In the first month the reference scenario results in a monthly rainfall sum of 30 mm, the dry scenario in 111 mm and the wet scenario in only 9 mm. Generally the model will always strive towards an equilibrium in its system states, which are a function of the model structure and parameters. In the scenario "wet" a lot of water is stored in the states of the model at the beginning, with the result, that little inverse rainfall is calculated. In the dry scenario on the other hand a higher amount of rainfall is estimated, since less water is stored in the states at the beginning. With time, however, the different inverse rainfall estimates will converge. In this time also the system states converge and after 9 months no differences are evident.

Similar to classical rainfall–runoff models formulated in a state-space approach, it is evident that cold states have a noteworthy influence on the simulation results. After an adequate spin-up time the system states however converge, leading to deterministic and unique inverse rainfall estimates.

5 Summary and conclusions

A calibrated rainfall–runoff model (forward model) reflects the catchment processes leading to runoff generation. Thus, inverting the model, i.e. calculating rainfall from runoff, yields the temporally disintegrated rainfall. In this paper we applied a conceptual rainfall–runoff model, which is inverted in an iterative approach, to simulate catchment rainfall from observed runoff. The estimated inverse rainfall is compared with two different rainfall realisations: apart of a ground observation, areal rainfall fields of the INCA-system are used. INCA is the meteorological nowcasting and analysis system developed and run by the Central Institute for Meteorology and Geodynamics of Austria (ZAMG) and is used for the majority of real-time flood forecasting systems in Austria.

In a first step, the forward model is calibrated with the ground observation and reproduces the dynamics and variability of the catchment responses to rainfall in a

HESSD
11, 13259–13309, 2014

satisfactory manner. Comparable model performance is also found in the validation period. These model parameters are then used for deriving catchment rainfall from runoff observations. The cumulative rainfall curves of the three rainfall realisations – ground observation (POBS), INCA, inverse rainfall (Inverse P) – are very similar, suggesting, that the inverse model is capable of representing the long-term quantitative rainfall conditions of the catchment. The correlation between Inverse P and POBS is higher or of the same magnitude compared to the correlation between POBS and INCA, suggesting that the inverse model also reflects the timing of rainfall in equal quality of INCA. Quantitative differences in the rainfall realisations evaluated with the mean squared error (MSE) show significant larger errors between POBS and Inverse P compared to POBS and INCA. Although the cumulative curves of the rainfall realisations are very similar, the higher variance of the inverse rainfall leads to the higher quantitative errors when evaluating the MSE. The higher variance to a great extent originates from a partial oscillating character of the inverse rainfall. Similar results are found for the validation period.

To test, if the inverse rainfall is conditioned by observed rainfall used as calibration input, additional model calibration is conducted using the INCA data as driving rainfall input for the forward model. The simulation of inverse rainfall on the basis of this model parameters set show very similar results as before, suggesting, that the inverse rainfall is not conditioned to the rainfall input used for model calibration.

Since the inverse model is formulated in a state-space approach additional simulations are performed with differing cold states at the beginning of the simulations. Here the results show, that the resulting inverse rainfall values converge to identical values after an adequate spin-up time.

It can be concluded that the application of the inverse model is a feasible approach to estimate mean areal rainfall values. The mean areal rainfall values can be used to enhance interpolated rainfall fields, e.g. for the estimation of rainfall correction factors or the parameterisation of elevation dependency. Furthermore, it is conceivable to use the inverse model in real-time flood forecasting systems, e.g. to gain additional information

HESSD
11, 13259–13309, 2014

on rainfall quantities. The estimation of areal rainfall leading to extreme flood events is afflicted with major uncertainties. Here the inverse modelling approach can be used as an additional information source concerning the rainfall conditions during extreme events.

In the presented work two different model parameter sets were used as a basis to calculate inverse rainfall. In a next step the influences and uncertainties in the inverse rainfall, which arise from different model parameters must be analysed systematically. With this analysis as a basis the application of the inverse model in ungauged basins is conceivable. Due to the lumped model setup only mean areal values of rainfall are calculated with the inverse model. The spatial disaggregation of the inverse areal rainfall estimates is therefore also an interesting future task.

Appendix A:

The forward model is formulated as follows, considering parameters and variables in Tables 2 and 3:

$$\mathrm{BWI}_t = \max(\min(\mathrm{INTMAX}, \mathrm{BWI}_{t-1} + R_t - \mathrm{ETp}_t), 0) \tag{A1}$$

$$\begin{aligned}\mathrm{BW0}_t &= \mathrm{BW0}_{t-1} + R_t - \mathrm{ETG}_t - Q1_t - Q2_t = \\ &\mathrm{BW0}_{t-1} + R_t - \min\left(\frac{\mathrm{BW0}_{t-1}}{\mathrm{FKFAK}\cdot M}, 1\right)\cdot \mathrm{ETp}_t \cdot \mathrm{ETVEGCOR} \\ &- R_t \cdot \left(\frac{\mathrm{BW0}_{t-1}}{M}\right)^{\mathrm{BETA}} - \mathrm{PEX2}\cdot \mathrm{BW0}_{t-1}\end{aligned} \tag{A2}$$

$$\begin{aligned}\mathrm{BW2}_t &= \mathrm{BW2}_{t-1} + Q2_t - \mathrm{QAB2}_t - \mathrm{QVS2}_t = \\ &\mathrm{BW2}_{t-1} + \mathrm{PEX2}\cdot \mathrm{BW0}_{t-1} - \alpha_2 \cdot \max(\mathrm{BW2}_{t-1} - H2, 0) - \beta_2 \cdot \mathrm{BW2}_{t-1}\end{aligned} \tag{A3}$$

$$\mathrm{BW3}_t = \mathrm{BW3}_{t-1} + \mathrm{QVS2}_t - \mathrm{QAB3}_t = \mathrm{BW3}_{t-1} + \beta_2 \cdot \mathrm{BW2}_{t-1} - \alpha_3 \cdot \mathrm{BW3}_{t-1} \tag{A4}$$

HESSD
11, 13259–13309, 2014

$$BW4_t = BW4_{t-1} + Q1_t + QAB2_t + QAB3_t - QSIM_t =$$
$$BW4_{t-1} + R_t \cdot \left(\frac{BW0_{t-1}}{M}\right)^{BETA} + \alpha_2 \cdot \max(BW2_{t-1} - H2, 0)$$
$$+ \alpha_3 \cdot BW3_{t-1} - \alpha_4 \cdot BW4_{t-1} \quad \text{(A5)}$$

with

$$\alpha_i = \frac{\Delta t}{TAB_i} \quad \text{and} \quad \text{(A6)}$$

$$\beta_i = \frac{\Delta t}{TVS_i}. \quad \text{(A7)}$$

TAB_i/TVS_i = recession coefficients. Δt modelling time step in units of hours.

The recession coefficient representing percolation processes in the soil layer exhibits a nonlinear characteristic and is calculated as a function of actual soil water content and a form parameter PEX2 [–]. This model concept reflects the fact, that higher soil moisture levels lead to higher soil permeability values. These induce higher percolation rates which are reflected by lower recession coefficients. The normalised curves in Fig. A1 are based on the equation for the soil-water content-pressure head curve presented by Van Genuchten (1980), where n in the original equation is represented by PEX2 [–].

References

Ahrens, B., Jasper, K., and Gurtz, J.: On ALADIN precipitation modeling and validation in an Alpine watershed, Ann. Geophys., 21, 627–637, doi:10.5194/angeo-21-627-2003, 2003.

Bergström, S.: The HBV model, in: Computer Models of Watershed Hydrology, edited by: Singh, V. P., Water Resources Publications, Highland Ranch, CO, USA, 443–476, 1995.

Bica, B., Herrnegger, M., Kann, A., and Nachtnebel, H. P.: HYDROCAST – Enhanced estimation of areal rainfallby combining a meteorological nowcasting system with a hydrologi-

HESSD
11, 13259–13309, 2014

cal model, Final report, Austrian Academy of Science, Vienna, doi:10.1553/hydrocast2011, 2011.
BMLFUW: Hydrological Atlas of Austria, 3rd Edn., Bundesministerium für Land- und Forstwirtschaft, Umwelt und Wasserwirtschaft, Wien, ISBN: 3-85437-250-7, 2007.
BMLFUW: Hydrographical Yearbook of Austria, Abteilung VII 3 – Wasserhaushalt im Bundesministerium für Land und Forstwirtschaft, Umwelt und Wasserwirtschaft, Wien, 2009.
Brent, R. P.: Algorithms for Minimization without Derivatives, Prentice-Hall, Englewood Cliffs, NJ, 1973.
de Jong, C., List, F., and Ergenzinger, C.: Experimental hydrological analyses in the Dischma based on daily and seasonal evaporation, Nord. Hydrol., 33, 1–14, 2002.
Di Baldassarre, G. and Montanari, A.: Uncertainty in river discharge observations: a quantitative analysis, Hydrol. Earth Syst. Sci., 13, 913–921, doi:10.5194/hess-13-913-2009, 2009.
Duan, Q., Sorooshian, S., and Gupta, V. K.: Effective and efficient global optimization for conceptual rainfall–runoff models, Water Resour. Res., 28, 1015–1031, 1992.
Eder, G., Fuchs, M., Nachtnebel, H. P., and Loibl, W.: Semi-distributed modelling of the monthly water balance in an alpine catchment, Hydrol. Process., 19, 2339–2360, 2005.
Elias, V., Tesar, M., and Buchtele, J.: Occult precipitation: sampling, chemical analysis and process modeling in the Sumava Mts. (Czech Republic) and in the Taunus Mts. (Germany), J. Hydrol., 166, 409–420, 1995.
Fekete, B. M., Vorosmarty, C. J., Roads, J. O., and Willmot, C. J.: Uncertainties in precipitation and their impacts on runoff estimates, J. Climate, 17, 294–304, 2004.
Groetsch, C.: Inverse Problems in Mathematical Sciences, Vieweg Mathematics for Scientists and Engineers, Wiesbaden, 1993.
Haiden, T. and Pistotnik, G.: Intensity-dependent parameterization of elevation effects in precipitation analysis, Adv. Geosci., 20, 33–38, doi:10.5194/adgeo-20-33-2009, 2009.
Haiden, T., Kann, A., Wittman, C., Pistotnik, G., Bica, B., and Gruber, C.: The Integrated Nowcasting through Comprehensive Analysis (INCA) system and its validation over the Eastern Alpine region, Weather Forecast., 26, 166–183, doi:10.1175/2010WAF2222451.1, 2011.
Hargreaves, G. H. and Samani, Z. A.: Estimating potential evapotranspiration, J. Irr. Drain. Div.-ASCE, 108, 225–230, 1982.
Herrnegger, M.: Zeitlich hochaufgelöste inverse Modellierung von Gebietsniederschlägen aus Abflussmessungen, PhD thesis, Institute of Water Management, Hydrology and Hydraulic Engineering, University of Natural Resources and Life Sciences, Vienna, Austria, 2013.

HESSD
11, 13259–13309, 2014

Herrnegger, M., Nachtnebel, H. P., and Haiden, T.: Evapotranspiration in high alpine catchments – an important part of the water balance!, Hydrol. Res., 43, 460–475, 2012.
Hino, M. and Hasabe, M.: Analysis of hydrologic characteristics from runoff data – a hydrologic inverse problem, J. Hydrol., 49, 287–313, 1981.
Jacobs, A. F. G., Heusinkveld, B. G., and Wichink Kruit, R. J.: Contribution of dew to the water budget of a grassland area in the Netherlands, Water Resour. Res., 42, W03415, doi:10.1029/2005WR004055, 2006.
Jasper, K. and Kaufmann, P.: Coupled runoff simulations as validation tools for atmospheric models at the regional scale, Q. J. Roy. Meteorol. Soc., 129, 673–692, 2007.
Jasper, K., Gurtz, J., and Lang, H.: Advanced flood forecasting in Alpine watersheds by coupling meteorological observations and forecasts with a distributed hydrological model, J. Hydrol., 267, 40–52, 2002.
Kirchner, J. W.: Catchments as simple dynamical systems: catchment characterization, rainfall–runoff modeling, and doing hydrology backward, Water Resour. Res., 45, W02429, doi:10.1029/2008WR006912, 2009.
Klemm, O. and Wrzesinski, T.: Fog deposition fluxes of water and ions to a mountainous site in Central Europe, Tellus, 59, 705–714, 2007.
Kling, H.: Spatio-temporal modelling of the water balance of Austria, Dissertation, University of Natural Resources and Applied Life Sciences, 234 pp., available at: http://iwhw.boku.ac.at/dissertationen/kling.pdf (last access: 7 October 2014), 2006.
Kling, H. and Nachtnebel, H. P.: A method for the regional estimation of runoff separation parameters for hydrological modelling, J. Hydrol., 364, 163–174, 2009.
Kling, H., Stanzel, P., Fuchs, M., and Nachtnebel, H. P.: Performance of the COSERO precipitation-runoff model under non-stationary conditions in basins with different climates, Hydrolog. Sci. J., doi:10.1080/02626667.2014.959956, in press, 2015.
Krajewski, W. F. and Smith, J. A.: Radar hydrology: rainfall estimation, Adv. Water Resour., 25, 1387–13, 2002.
Krajewski, W. F., Villarini, G., and Smith, J. A.: RADAR-rainfall uncertainties, B. Am. Meteorol. Soc., 91, 87–94, doi:10.1175/2009BAMS2747.1, 2010.
Krier, R., Matgen, P., Goergen, K., Pfister, L., Hoffmann, L., Kirchner, J. W., Uhlenbrook, S., and Savenije, H. H. G.: Inferring catchment precipitation by doing hydrology backward: a test in 24 small and mesoscale catchments in Luxembourg, Water Resour. Res., 48, W10525, doi:10.1029/2011WR010657, 2012.

HESSD
11, 13259–13309, 2014

Kuczera, G., Kavetski, D., Franks, S., and Thyer, M.: Towards a Bayesian total error analysis of conceptual rainfall–runoff models: characterising model error using storm-dependent parameters, J. Hydrol., 331, 161–177, 2006.

Kunstmann, H. and Stadler, C.: High resolution distributed atmospheric-hydrological modeling for Alpine catchments, J. Hydrol., 314, 105–124, 2005.

McMillan, H., Freer, J., Pappenberger, F., Krueger, T., and Clark, M.: Impacts of uncertain river flow data on rainfall–runoff model calibration and discharge predictions, Hydrol. Process., 24, 1270–1284, oi:10.1002/Hyp.7587, 2010.

Nachtnebel, H. P., Baumung, S., and Lettl, W.: Abflussprognosemodell für das Einzugsgebiet der Enns und Steyr, report, Institute of Water Management, Hydology and Hydraulic Engineering, University of Natural Resources and Applied Life Sciences, Vienna, Austria, 1993.

Nash, J. E. and Sutcliffe, J. V.: River flow forecasting through conceptual models, Part I: A discussion of principles, J. Hydrol., 10, 282–290, 1970.

Pappenberger, F., Matgen, P., Beven, K. J., Henry, J. B., Pfister, L., and de Fraipont, P.: Influence of uncertain boundary conditions and model structure on flood inundation predictions, Adv. Water Resour., 29, 1430–1449, 2006.

Pelletier, M. P.: Uncertainties in the determination of river discharge: a literature review, Can. J. Civil Eng., 15, 834–850, 1987.

Perrin, C., Michel, C., and Andréassian, V.: Does a large number of parameters enhance model performance? Comparative assessment of common catchment model structures on 429 catchments, J. Hydrol., 242, 275–301, 2001.

Press, W. H., Teukolsky, S. A., Vetterling, W. T., and Flannery, B. P.: Numerical Recipes in FORTRAN, The Art of Scientific Computing, Cambridge Univ. Press, New York, 965 pp., 1992.

Seibert, J. and Morén, A.-S.: Reducing systematic errors in rainfall measurements using a new type of gauge, Agr. Forest Meteorol., 98–99, 341–348, 1999.

Sevruk, B.: Methodische Untersuchungen des systematischen Messfehlers der Hellmann-Regenmesser im Sommerhalbjahr in der Schweiz, dissertation, Eidgenöss. Techn. Hochsch. Zürich, Zürich, Switzerland, 1981.

Sevruk, B.: Correction of precipitation measurements. Proc. Workshop on the Correction of Precipitation Measurements, in: Zürcher Geographische Schriften, ETH Zurich, Zurich, p. 289, 1986.

HESSD
11, 13259–13309, 2014

Sevruk, B. and Nespor, V.: Empirical and theoretical assessment of the wind induced error of rain measurement, Water Sci. Technol., 37, 171–178, 1998.
Simoni, S., Padoan, S., Nadeau, D. F., Diebold, M., Porporato, A., Barrenetxea, G., Ingelrest, F., Vetterli, M., and Parlange, M. B.: Hydrologic response of an alpine watershed: application of a meteorological wireless sensor network to understand streamflow generation, Water Resour. Res., 47, W10524, doi:10.1029/2011WR010730, 2011.
Stanzel, P., Kahl, B., Haberl, U., Herrnegger, M., and Nachtnebel, H. P.: Continuous hydrological modeling in the context of real time flood forecasting in alpine Danube tributary catchments, IOP Conf. Ser., 4, 012005, doi:10.1088/1755-1307/4/1/01200, 2008.
Sugawara, M.: On the weights of precipitation stations, in: Advances in Theoretical Hydrology, edited by: O'Kane, J. P., Elsevier Science Publishers, Amsterdam, 59–74, 1992.
Tarantola, A.: Inverse Problem Theory and Methods for Model Parameter Estimation, Society for Industrial and Applied Mathematics, Philadelphia, 352 pp., 2005.
Valéry, A., Andréassian, V., and Perrin, C.: Inverting the hydrological cycle: when streamflow measurements help assess altitudinal precipitation gradients in mountain areas, in: New Approaches to Hydrological Prediction in Data-sparse Regions, IAHS Publ., 333, 281–286, 2009.
Valéry, A., Andréassian, V., and Perrin, C.: Regionalisation of rainfall and air temperature over high-altitude catchments – learning from outliers, Hydrolog. Sci. J., 55, 928–940, 2010.
van Genuchten, M. T.: A closed-form equation for predicting the hydraulic conductivity of unsaturated soils, Soil Sci. Soc. Am. J., 44, 892–898, 1980.
Vrugt, J. A., ter Braak, C. J. F., Clark, M. P., Hyman, J. M., and Robinson, B. A.: Treatment of input uncertainty in hydrologic modeling: doing hydrology backward with Markov chain Monte Carlo simulation, Water Resour. Res., 44, W00B09, doi:10.1029/2007WR006720, 2008.
Wood, S. J., Jones, D. A., and Moore, R. J.: Accuracy of rainfall measurement for scales of hydrological interest, Hydrol. Earth Syst. Sci., 4, 531–543, doi:10.5194/hess-4-531-2000, 2000.

HESSD
11, 13259–13309, 2014

Table 1. Magnitude of different systematic errors in precipitation measurements.

Systematic error	Magnitude
Wind-induced errors	2–10 % (liquid precipitation) 10 –> 50 % (snow)
Wetting losses	2–10 %
Evaporation losses	0–4 %
Splash-out and splash-in	1–2 %
Flog and dew	4–10 %

HESSD
11, 13259–13309, 2014

Table 2. Model parameters θ_i.

Parameter	Units	Range	Description
INTMAX	mm	0.5–2.5	Interception storage capacity
M	mm	80–250	Soil storage capacity
FKFAK	–	0.5–1	Critical soil moisture for actual evapotranspiration
ETVEGCOR	–	0.4–1.1	Vegetation correction factor for actual evapotranspiration from soil
BETA	–	0.1–10	Exponent for computing fast runoff generation
KBF	h	4000–12 000	Recession coefficient for percolation from soil module
PEX2	–	5–25	Parameter for non-linear percolation
TAB2	h	50–500	Recession coefficient for interflow
TVS2	h	50–500	Recession coefficient for percolation from interflow reservoir
H2	mm	0–25	Outlet height for interflow
TAB3	h	1000–5000	Recession coefficient for base flow
TAB4	h	0.05–10	Recession coefficient for routing

HESSD
11, 13259–13309, 2014

Table 3. Model fluxes and system states S_i.

Variable	Units	Type	Description
R	mm	Input	Rainfall
ETp	mm	Input	Potential evapotranspiration
ETI	mm	Output	Actual Evapotranspiration from interception module
ETG	mm	Output	Actual Evapotranspiration from soil module
BWI	mm	State	Water stored in interception module
BW0	mm	State	Water stored in soil module
BW2	mm	State	Water stored in interflow reservoir
BW3	mm	State	Water stored in base flow reservoir
BW4	mm	State	Water stored in routing reservoir
R_Soil	mm	Internal flux	Input into soil module
Q1	mm	Internal flux	Fast runoff from soil module
Q2	mm	Internal flux	Percolation from soil module
QAB2	mm	Internal flux	Interflow
QVS2	mm	Internal flux	Percolation from interflow reservoir
QAB3	mm	Internal flux	Base flow
QSIM	mm	Output	Total runoff

HESSD
11, 13259–13309, 2014

Table 4. Characteristics of the study catchment (BMLFUW, 2007; BMLFUW, 2009).

Basin area [km^2]	38.4
Mean elevation [m]	598
Elevation range [m]	413–1511
Mean annual precipitation [mm]	1345
Mean annual runoff [$m^3 s^{-1}$]	1.12

HESSD
11, 13259–13309, 2014

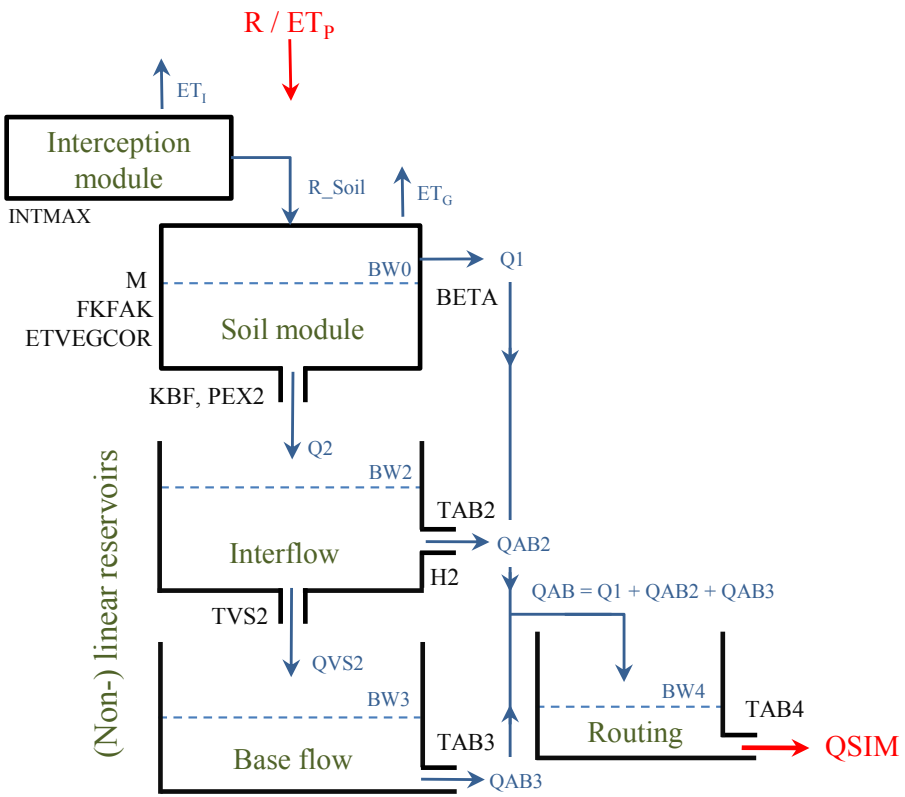

Figure 1. Structure, parameters and states of the forward model.

HESSD
11, 13259–13309, 2014

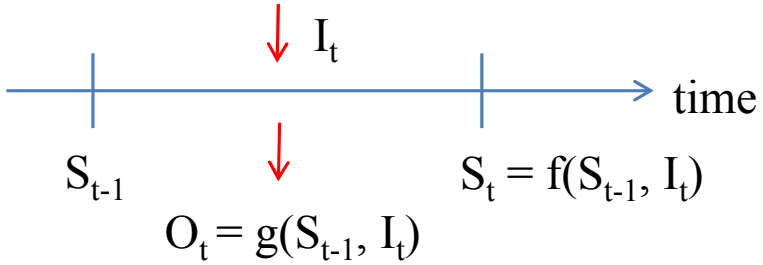

Figure 2. Schematic representation of the state space approach with system states *S*, Input *I*, Output *O* and time component *t*.

HESSD
11, 13259–13309, 2014

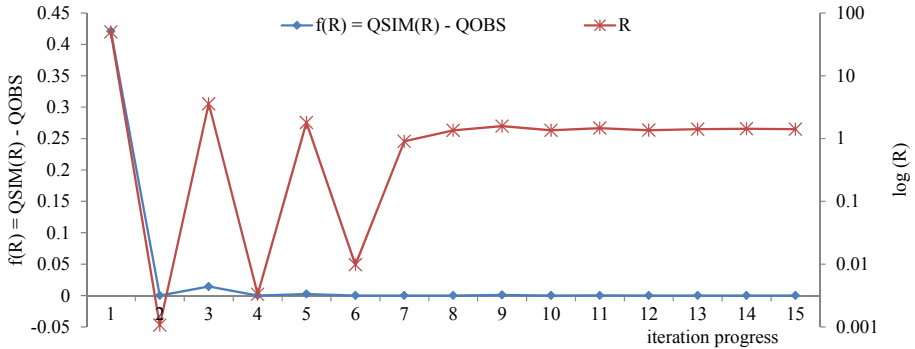

Figure 3. Illustration of the iteration progress for one model time step. Note that the right *y* axis showing the inverse rainfall values (*R*) is in a logarithmic scale.

HESSD
11, 13259–13309, 2014

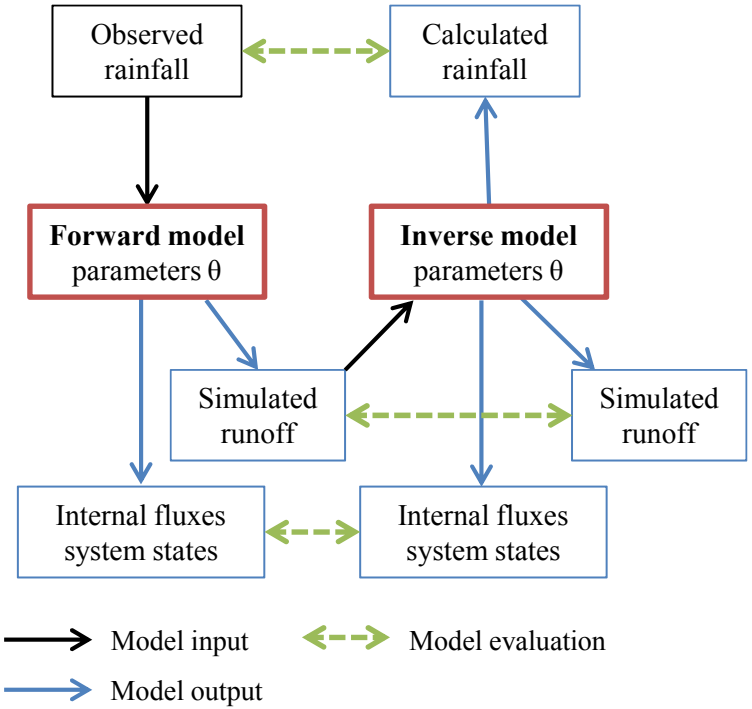

Figure 4. Setup of the virtual experiments and evaluation of the inverse model. All variables are calculated for every Monte Carlo run, in which parameters θ are varied.

HESSD
11, 13259–13309, 2014

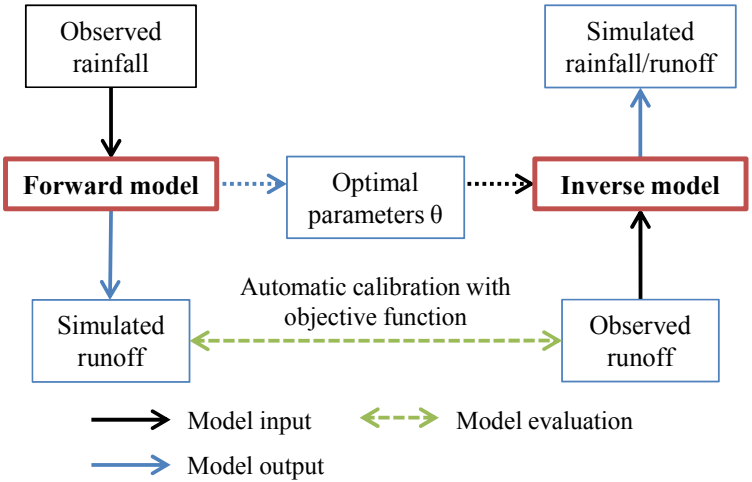

Figure 5. Parameter estimation and calculation scheme.

HESSD
11, 13259–13309, 2014

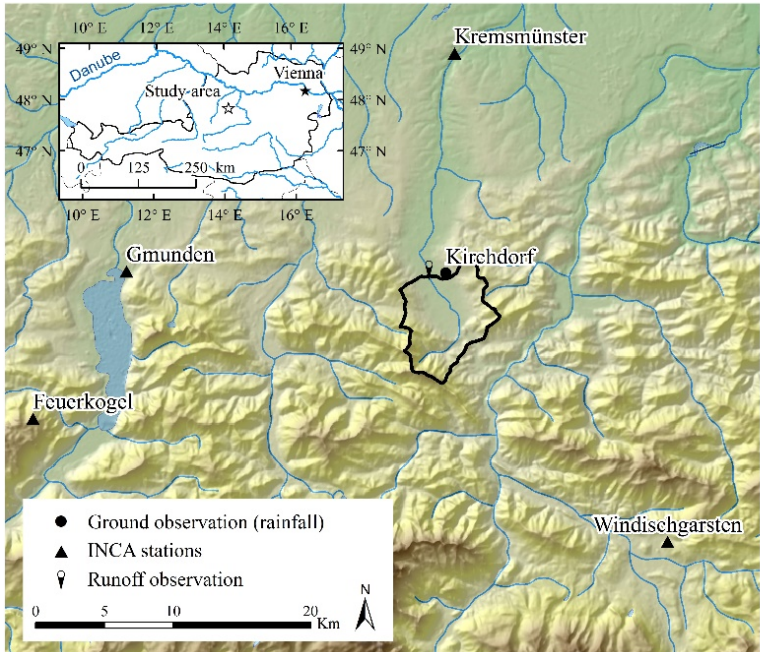

Figure 6. Krems catchment and location of meteorological stations.

HESSD
11, 13259–13309, 2014

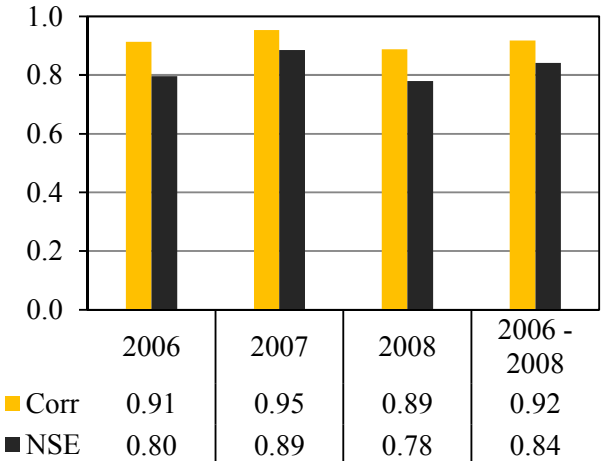

Figure 7. Model performance for the calibration period expressed by correlation (CORR) and Nash–Sutcliffe-Efficiency (NSE).

HESSD
11, 13259–13309, 2014

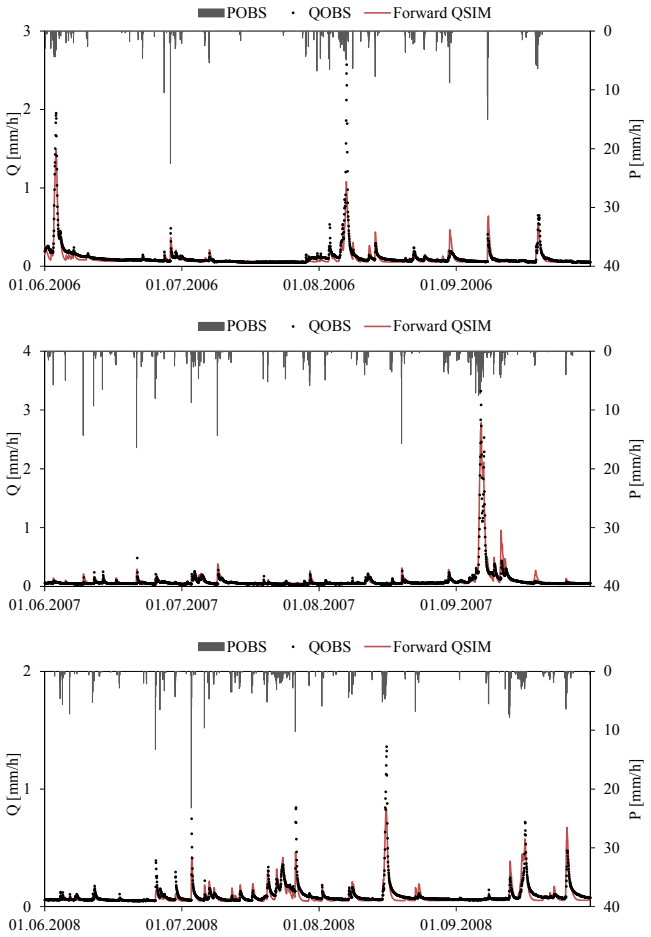

Figure 8. Observed (QOBS) and simulated runoff of the forward model (Forward QSIM) for the calibration periods. Ground observation of rainfall (POBS) used as input is also shown.

HESSD
11, 13259–13309, 2014

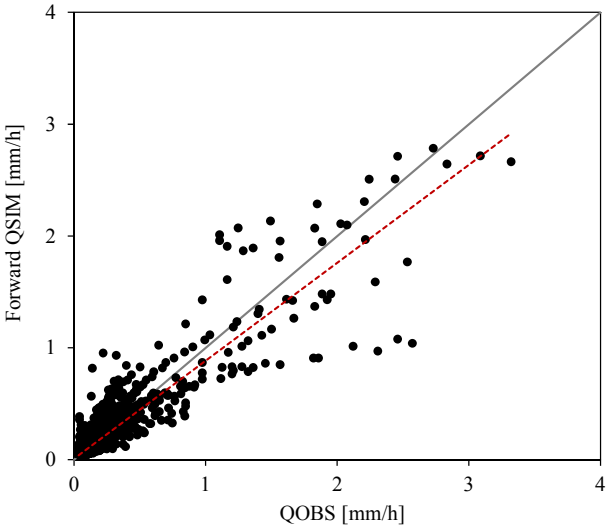

Figure 9. Scatterplot between observed (QOBS) and simulated runoff (Forward QSIM) for the calibration period, including the dotted regression line.

HESSD
11, 13259–13309, 2014

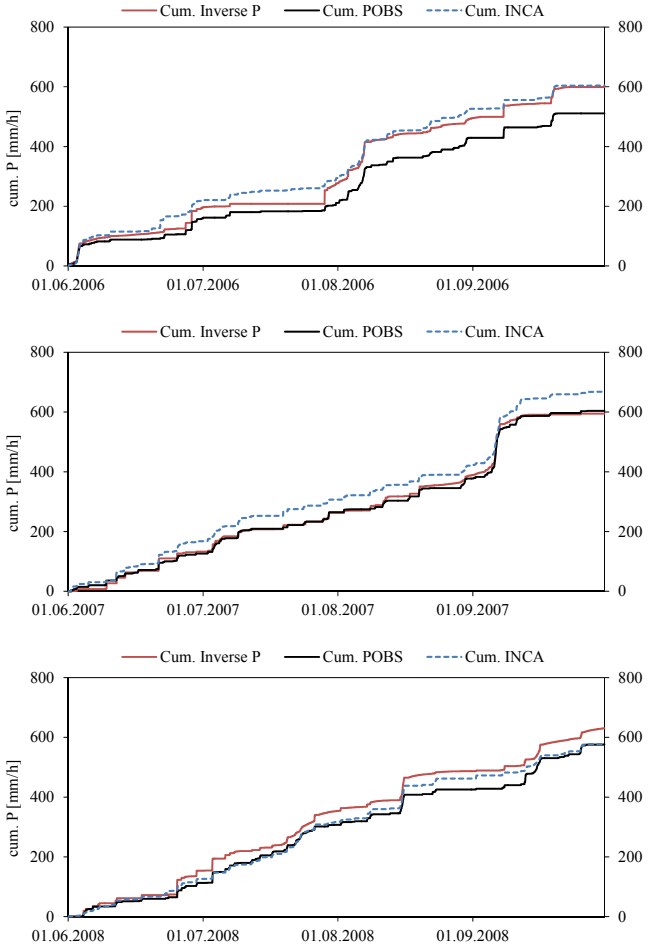

Figure 10. Cumulative rainfall curves for inverse, observed and INCA-rainfall for the periods in 2006, 2007 and 2008.

HESSD
11, 13259–13309, 2014

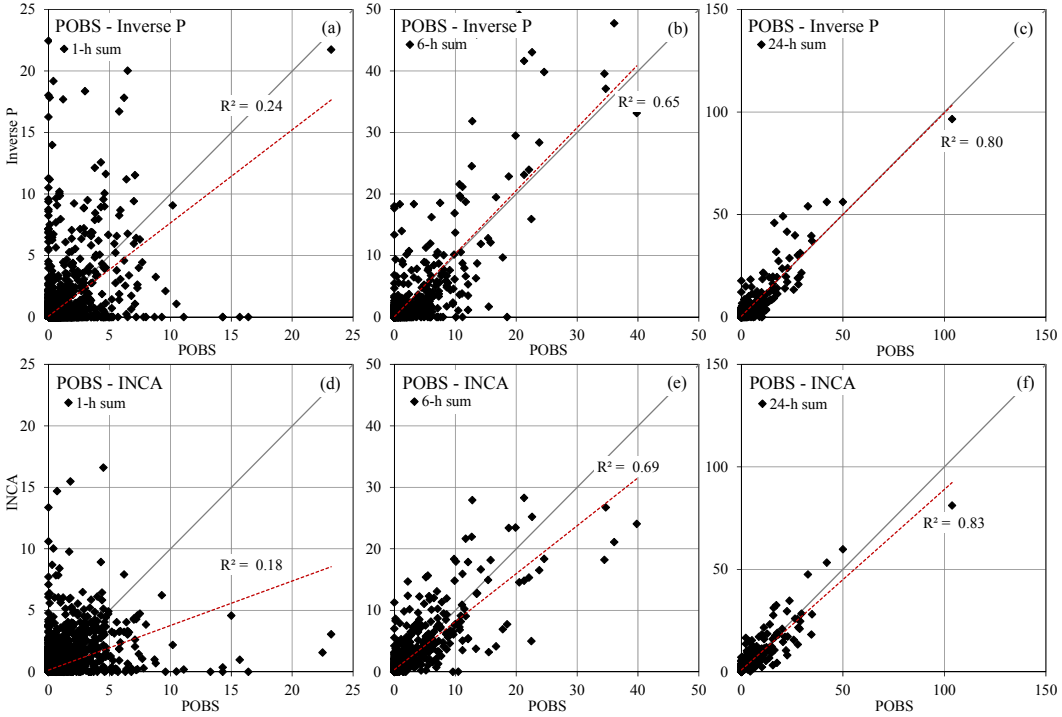

Figure 11. Scatterplot between station data (POBS) and inverse rainfall (Inverse P) (upper row panels) and INCA-data (lower row panels) for 1, 6 and 24 h sums.

HESSD
11, 13259–13309, 2014

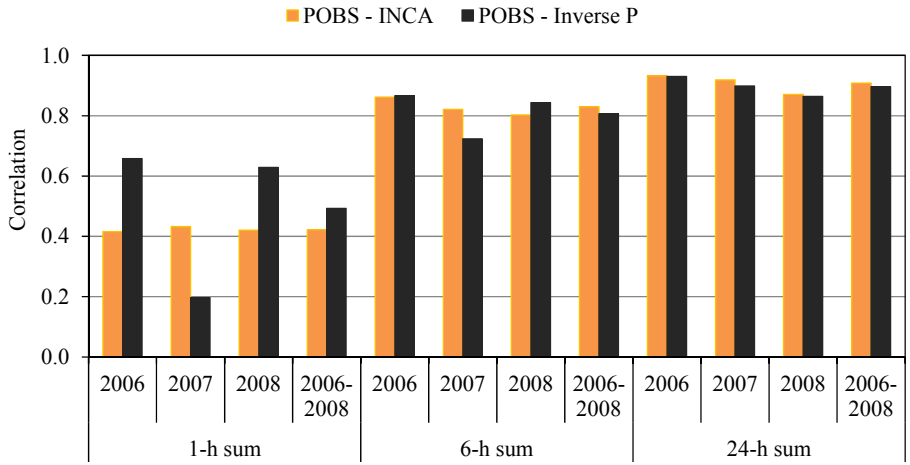

Figure 12. Correlation between different rainfall realisations and for different evaluation periods and temporal aggregation lengths.

HESSD
11, 13259–13309, 2014

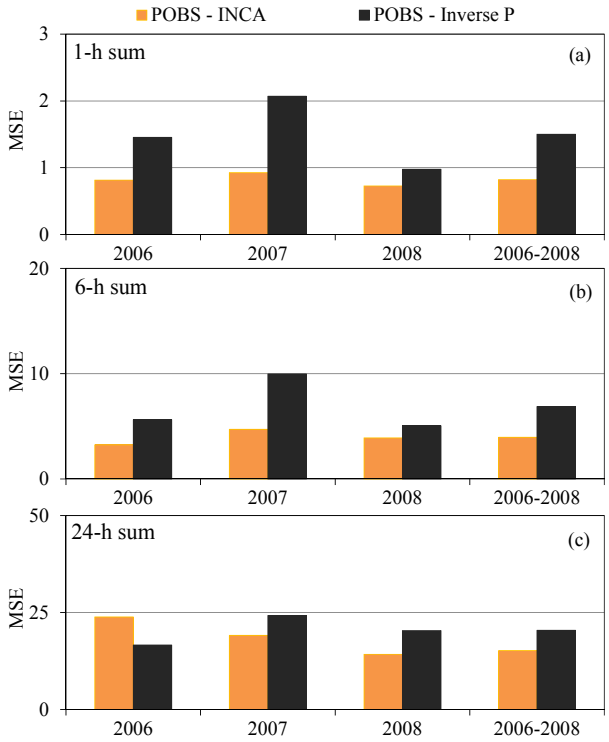

Figure 13. Mean squared error (MSE) between different rainfall realisations and temporal aggregation lengths.

HESSD
11, 13259–13309, 2014

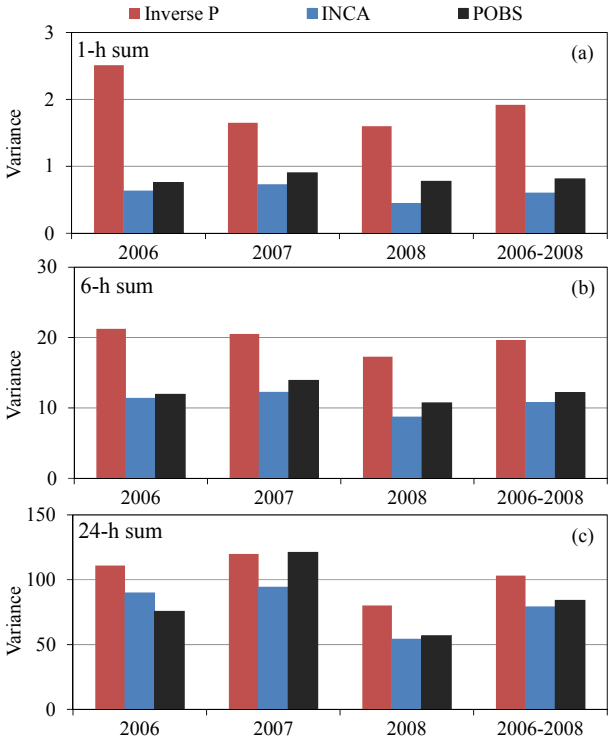

Figure 14. Variance for different rainfall realisations and temporal aggregation lengths.

HESSD
11, 13259–13309, 2014

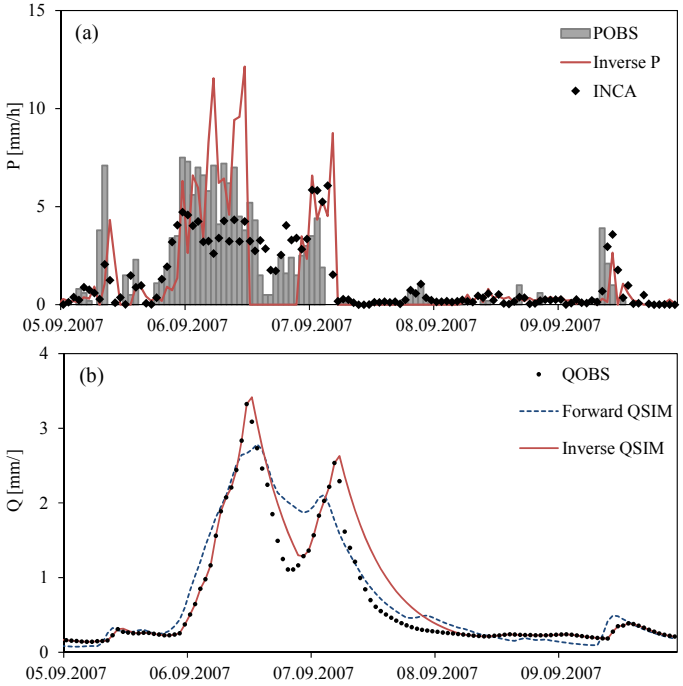

Figure 15. Temporal development of the different rainfall realisations **(a)** and runoff **(b)** for a flood event.

HESSD
11, 13259–13309, 2014

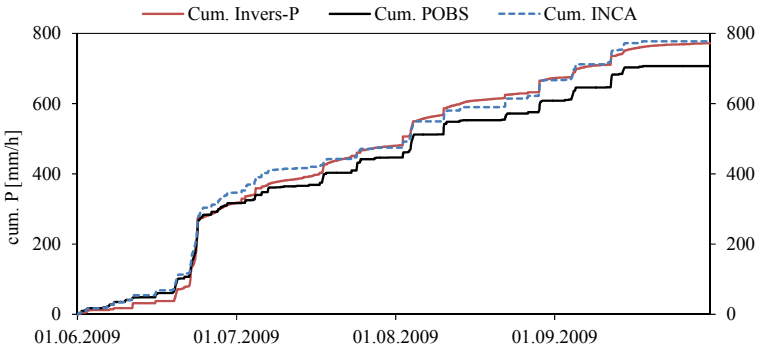

Figure 16. Cumulative rainfall curves for inverse, observed and INCA-rainfall for the independent period in 2009.

HESSD
11, 13259–13309, 2014

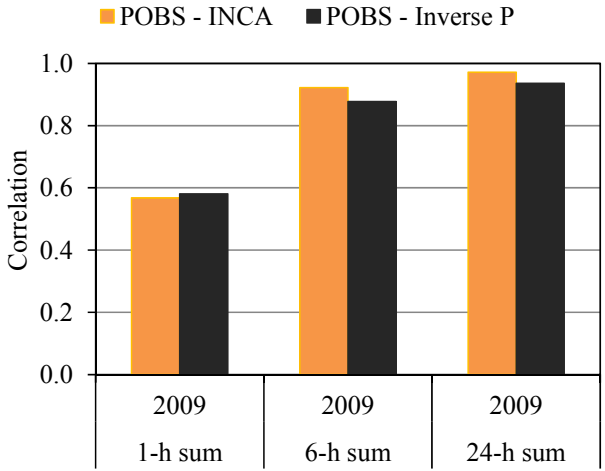

Figure 17. Correlation between different rainfall realisations in den independent validation period 2009 and temporal aggregation lengths.

HESSD
11, 13259–13309, 2014

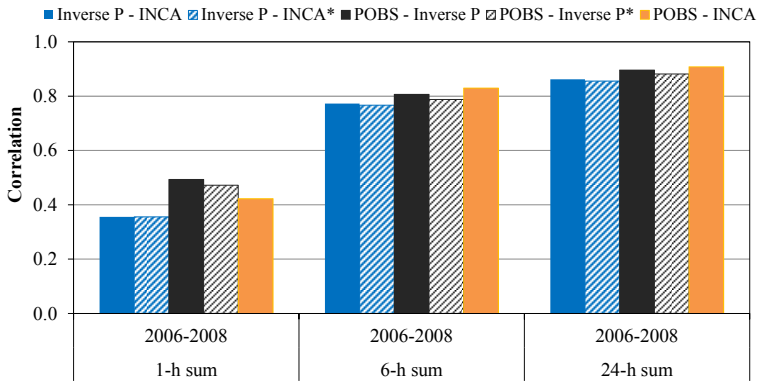

Figure 18. Correlation between different rainfall realisations and temporal aggregation lengths. Data marked with an asterisk (∗) is based on the calibration with INCA-data as input.

HESSD
11, 13259–13309, 2014

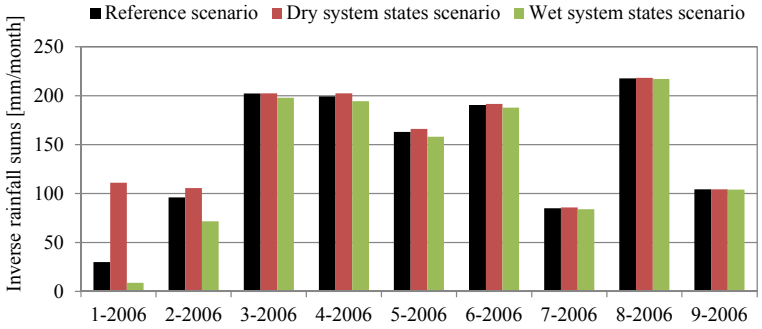

Figure 19. Monthly sums of inverse rainfall simulated in the scenarios "reference", "dry" and "wet".

HESSD
11, 13259–13309, 2014

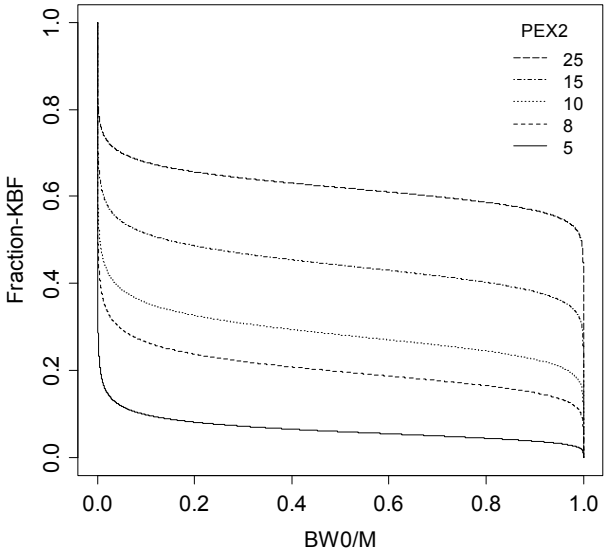

Figure A1. Fraction of parameter KBF as a function of relative soil water content (BW0/M) and the parameter PEX2.

HESSD
11, 13259–13309, 2014